# Interlayer Potential for Graphene/h-BN Heterostructures

Itai Leven,[†] Tal Maaravi,[†] Ido Azuri,[‡] Leeor Kronik,[‡] and Oded Hod*,[†]

[†]Department of Physical Chemistry, School of Chemistry, The Raymond and Beverly Sackler Faculty of Exact Sciences and The Sackler Center for Computational Molecular and Materials Science, Tel Aviv University, Tel Aviv 6997801, Israel

[‡]Department of Materials and Interfaces, Weizmann Institute of Science, Rehovoth 76100, Israel

Ⓢ Supporting Information

ABSTRACT: We present a new force-field potential that describes the interlayer interactions in heterojunctions based on graphene and hexagonal boron nitride (h-BN). The potential consists of a long-range attractive term and a short-range anisotropic repulsive term. Its parameters are calibrated against reference binding and sliding energy profiles for a set of finite dimer systems and the periodic graphene/h-BN bilayer, obtained from density functional theory using a screened-exchange hybrid functional augmented by a many-body dispersion treatment of long-range correlation. Transferability of the parametrization is demonstrated by considering the binding energy of bulk graphene/h-BN alternating stacks. Benchmark calculations for the superlattice formed when relaxing the supported periodic heterogeneous bilayer provide good agreement with both experimental results and previous computational studies. For a free-standing bilayer we predict a highly corrugated relaxed structure. This, in turn, is expected to strongly alter the physical properties of the underlying monolayers. Our results demonstrate the potential of the developed force-field to model the structural, mechanical, tribological, and dynamic properties of layered heterostructures based on graphene and h-BN.
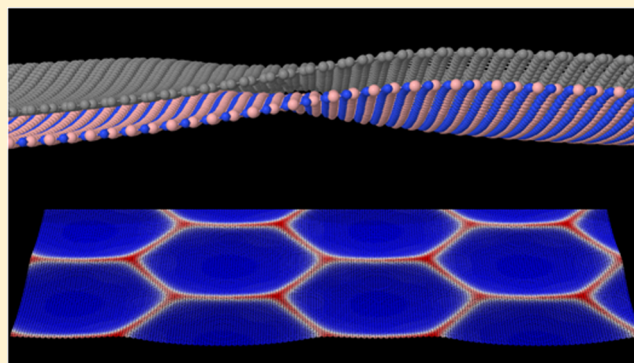
■ INTRODUCTION

In recent years two-dimensional heterostructures, formed by stacking different single-layered materials, have gained much attention due to their uniquely tailored physical properties.[1−4] The heterojunction of graphene and hexagonal boron nitride (h-BN) is probably the most prominent member of this family, exhibiting rich physical properties that include a tunable band gap,[5−8] ultrahigh electron mobility,[9−11] the appearance of Hofstadter's butterfly phenomenon,[12,13] and the demonstration of controllable hyperbolic metamaterial characteristics.[14] Due to the intrinsic lattice constant mismatch between graphene and h-BN, graphene tends to deform when placed on an h-BN substrate, thus adapting itself to the underlying lattice.[8,15] This, in turn, was shown to alter its electronic and optical properties, opening new venues for technological applications.[7,16−18] Another important realm where such heterojunctions play a central role is the field of nanotribology. Here, it was predicted that the flat graphene/h-BN interface (as well as related two-dimensional junctions) formed at the junction of the corresponding multilayered materials, namely graphite and bulk h-BN, should exhibit robust superlubricity that may reduce friction and wear in nano (electro-)mechanical systems.[19−22]

Theory and computation may provide valuable insights for the design of such novel two-dimensional heterostructures and for the interpretation of their measured properties.[17,19,23−28] To this end, an accurate description of the interlayer interactions is an essential requirement from any computational method used for modeling these systems.[7,15,16,26,29−34] The interlayer potential in layered materials can be generally decomposed into two main contributions: (i) long-range attractive interactions and (ii) short-range repulsive interactions. The long-range term results from dispersion interactions and possibly also electrostatic contributions and is the driving force for the interlayer adhesion.[22,35−37] The short-range term originates mainly from Pauli repulsions between overlapping electron clouds of atoms residing on adjacent layers and is the dominant factor in determining the interlayer sliding energy corrugation.[19,23−25,35,38] The balance between these two contributions determines the equilibrium interlayer distance and the overall binding energy of the layered structure.[37]

In the homogeneous bilayer graphene and bilayer h-BN systems, it was found that the short-range Pauli repulsions introduce an anisotropy that cannot be described simply by two-body potentials that depend solely on the interatomic distance.[39,40] Hence, the standard Lennard-Jones term that provides decent binding characteristics at a given stacking mode severely underestimates the overall sliding energy landscape corrugation in these materials.[41] To account for this, dedicated registry dependent interlayer force-fields have been developed, which simultaneously capture the adhesion and anisotropic
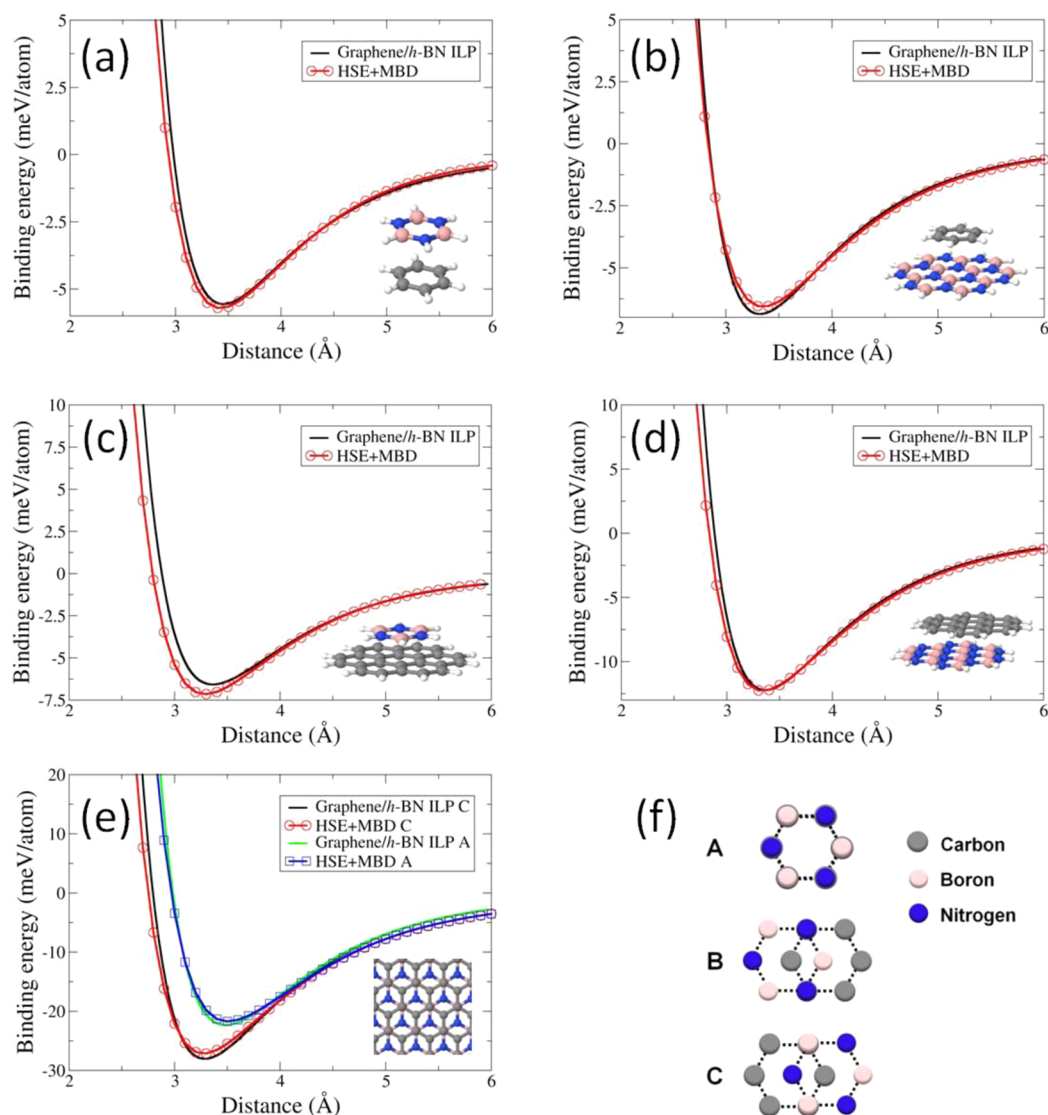
Figure 1. Binding energy curves for the (a) benzene/borazine dimer; (b) benzene on HBNC; (c) borazine on coronene; (d) coronene/HBNC dimer; and (e) periodic graphene/*h*-BN bilayer calculated at the optimal C stacking mode (see panel (f)), obtained from HSE+MBD (open red circles) and from the graphene/*h*-BN ILP developed in this work (full black line). Schematic representations of the corresponding systems are included as insets in each panel. For the periodic system (panel (e)) the binding energy curve at the worst (A) stacking configuration is presented as well. Panel (f) presents the high symmetry stacking modes of the graphene/*h*-BN heterojunction. For the finite systems the calculated binding energies were divided by the total number of atoms in the dimer (including hydrogen atoms), and for the periodic systems they were divided by the total number of atoms per unit-cell. Reference energies of the finite systems were calculated at an intermonomer distance of 100 Å. Reference energies of the infinite bilayer were taken as the sum of individual monomer contributions.

repulsive characteristics of the interlayer interaction in these homogeneous junctions.[39,40]

In the present paper, we develop an anisotropic interlayer potential for the heterogeneous interface of graphene and *h*-BN. To this end, we adopt the functional form of the recently reported interlayer potential (ILP) for hexagonal boron nitride (*h*-BN).[40] The force-field parametrization is performed against interlayer binding and sliding energy results obtained via state-of-the-art density functional theory (DFT) calculations utilizing a screened-exchange hybrid functional augmented by many-body dispersion treatment of long-range correlation.[42,43] Transferability of the parametrization is demonstrated by considering the binding energy of bulk graphene/*h*-BN alternating stacks. We further benchmark the developed force-field by studying the structural properties of large-scale graphene/*h*-BN surfaces, known to form commensurate regions

separated by domain walls.[15] This result has been previously rationalized based on continuum models and empirical force-fields.[7,26,31] Here, we obtain it in a predictive manner using an atomistic force-field derived from first-principles calculations.

DESCRIPTION OF THE FORCE-FIELD

In addition to long-range attractive dispersive and short-range repulsive interactions, the *h*-BN ILP,[40] on which the potential developed here is based, contained another term reflecting classical monopolar *electrostatic* interactions between partially charged ionic lattice sites residing on different layers. In the case of the graphene/*h*-BN heterojunction, this would be relevant only if there is significant induced polarization of the C−C bonds in graphene due to the polarized nature of the heteronuclear B−N bonds in the adjacent *h*-BN layer.

However, as the electrostatic potential decays exponentially with the distance from the *h*-BN surface[37,44] the net effect is expected to be quite weak. This has been confirmed by observing insignificant Hirshfeld charges ($\sim$0.005e) on the carbon atoms at the graphene/*h*-BN heterojunction, using the DFT calculations described below. Therefore, we discard the interlayer electrostatic interaction term and recalibrate the long-range dispersion attraction and short-range repulsion terms for this system. A full account of the latter two terms can be found in ref 40. Here, we provide a brief description of their functional form, for completeness.

Long-Range Attractive Term. The long-range attractive term of our interlayer force-field is based on the form of the Tkatchenko-Scheffler dispersion correction scheme to DFT.[45] In this approach, standard semilocal or hybrid exchange-correlation density functional approximations that fail to describe long-range van der Waals (vdW) interactions are augmented by asymptotic pairwise terms that decay as c_6/r^6 with the interatomic distance, r. These terms are damped at short distances to avoid double-counting of short-range correlation effects.

In our interlayer force-field, these pairwise long-range attraction terms take the form

$$E_{\text{Att}}(r_{ij}) = \text{Tap}(r_{ij})\left\{ -\frac{1}{1 + e^{-d[(r_{ij}/(s_R \cdot r_{ij}^{\text{eff}}))-1]}} \cdot \frac{C_{6,ij}}{r_{ij}^6} \right\} \tag{1}$$

Here, r_{ij} is the distance between a pair of atoms, i and j, located on adjacent layers, r_{ij}^{eff} is the sum of effective equilibrium vdW atomic radii of the pair, $C_{6,ij}$ is the pairwise dispersion coefficient of the two atoms in the molecular or solid-state environment, and d and s_R are unit-less parameters defining the steepness of the short-range Fermi-type damping function and its onset, respectively. The term in the curly parentheses is identical in form to the Tkatchenko-Scheffler one.[45] For computational efficiency we further damp it at large distances using a taper function[46] of the form

$$\text{Tap}(r_{ij}) = \frac{20}{R_{\text{cut}}^7}r_{ij}^7 - \frac{70}{R_{\text{cut}}^6}r_{ij}^6 + \frac{84}{R_{\text{cut}}^5}r_{ij}^5 - \frac{35}{R_{\text{cut}}^4}r_{ij}^4 + 1$$

which provides a continuous (up to third derivative) cutoff for interatomic separations larger than R_{cut}.[47]

Short-Range Repulsive Term. We follow the approach developed by Kolmogorov and Crespi (KC)[39] for graphene to describe the short-range anisotropic interlayer repulsive interactions. In this scheme, the repulsive term between two atoms i and j on adjacent layers is defined not only as a function of their interatomic distance, r_{ij}, but also as a function of their pairwise transverse distance, ρ_{ij}. The latter, which is required to capture the anisotropy of the interatomic repulsion, is defined as the shortest distance between atom j on one layer and the surface normal at the position of atom i in the adjacent layer. The surface normal itself is taken as a vector perpendicular to the triangle formed by the three nearest neighbors of atom i. Full details regarding the calculation of the surface normal and the lateral distance can be found in refs 40 and 28. With this, the overall expression describing the repulsive interaction is given by

$$E_{\text{Rep}}(r_{ij}, \rho_{ij}) = \text{Tap}(r_{ij})e^{\alpha_{ij}\left(1-\frac{r_{ij}}{\beta_{ij}}\right)}\left[\varepsilon_{ij} + C_{ij}\left(e^{-(\rho_{ij}/\gamma_{ij})^2} + e^{-(\rho_{ji}/\gamma_{ij})^2}\right)\right] \tag{2}$$

where ε_{ij} and C_{ij} are energy constants associated with the isotropic and anisotropic repulsion, respectively, β_{ij} and γ_{ij} set the corresponding interaction ranges, and α_{ij} sets the steepness of the isotropic term.

PARAMETERIZATION

Reference DFT Calculations. The above-described graphene/*h*-BN ILP has been parametrized against a series of sliding and binding energy calculations for finite and periodic heterogeneous bilayer models, obtained from DFT. A total of five systems (see insets of Figure 1) were used as reference for the binding energy curves calculations: the benzene/borazine dimer, benzene atop hexaborazino-coronene (the BN analogue of coronene, with the chemical formula $B_{12}N_{12}H_{12}$, denoted here as HBNC), borazine atop coronene ($C_{24}H_{12}$), the coronene/HBNC dimer, and the periodic graphene/*h*-BN bilayer.[48] Two of these systems were further used for sliding energy landscape reference calculations: the finite benzene/HBNC system and the periodic graphene/*h*-BN bilayer system.

All reference data were obtained from dispersion-corrected DFT calculations. A major advantage of this approach is that the difficult problem of obtaining an accurate description of both geometry and electronic structure can be generally overcome by decoupling the two issues:[49] an exchange-correlation functional that is appropriate for the electronic structure problem, but does not include a good description of dispersive interactions, is augmented with first-principles dispersion corrections. The screened-exchange hybrid functional of Heyd, Scuseria, and Ernzerhof (HSE)[50–53] has been established previously to be successful in describing the electronic properties of graphene, *h*-BN, and their hybrid structures (see, e.g., refs 35, and 54–59). Augmenting HSE with simple pairwise dispersion corrections is known to be insufficient for carbon-based nanostructures in general, and graphene in particular, owing to screening effects.[60] Therefore, we employ many-body dispersion (MBD) corrections.[42,43] Briefly, in this approach one starts by evaluating the Tkatchenko-Scheffler C_6 coefficients and atomic polarizabilities, obtained from normalizing their free-atom values based on the effective atomic Hirshfeld volume in the molecular or solid-state environment. Next, the atomic response functions are mapped into a set of quantum harmonic oscillators. These are then coupled through dipole–dipole interactions to obtain self-consistently screened polarizabilities, which are used to obtain the correlation energy of the interacting oscillator model system, within the random-phase approximation. Here, we use the range-separated version of this scheme,[43] in which double-counting of correlation is minimized by using short-range dipole–dipole interaction for the self-consistent screening but long-range interaction for the calculation of the correlation energy. This approach has been found to be quantitatively useful for systems as diverse as molecular complexes, molecular solids, layered materials, and adsorbates on metal surfaces,[43,61–65] including, importantly, the graphene bilayer,[43,64] multilayered hexagonal boron nitride and graphene,[22] a graphene sheet adsorbed on the Ag(111) surface,[63] and bulk graphite and *h*-BN.[64] Furthermore, using this approach we obtained bilayer graphene and *h*-BN binding energies of 24.6 and 27.3 meV/atom. These values are $\sim$7 meV/atom higher than corresponding quantum Monte Carlo results—a considerably better agreement than that obtained with standard dispersion-corrected DFT approaches.[66,67] We therefore view the combination of the HSE functional with MBD corrections,

denoted henceforth as HSE+MBD, as a state-of-the art DFT approach, providing a good balance of accuracy and complexity for computing binding energy curves and sliding energy landscapes, against which the ILP developed here is parametrized and subsequently benchmarked.

Individual monomers of graphene and *h*-BN were first optimized using the HSE functional and the split-valence double-ζ 6-31G** Gaussian basis set,[68] as implemented in the GAUSSIAN suite of programs.[69] For all dimer systems considered, the optimized monomers were then stacked at the optimal (C) configuration (see Figure 1f) to form the bilayer systems. For the periodic bilayer system (panel (e)), the optimized monomers were additionally stacked at the worst (A) stacking configuration (see Figure 1f). All system calculations were then pursued using HSE+MBD with the tier-2 basis set,[70] as implemented in the FHI-AIMS suite of programs,[71] using tight convergence settings (see the Supporting Information for more details). Basis set superposition errors at the equilibrium interdimer distance with this basis set are estimated to be of the order of 0.1 meV/atom (see the Supporting Information) and are therefore neglected throughout the parametrization procedure.[35,49] The systems were rigidly shifted vertically, allowing for binding-energy calculations to be carried out at each interlayer distance, as shown in Figures 1 and 2 . Sliding energy profiles, obtained for
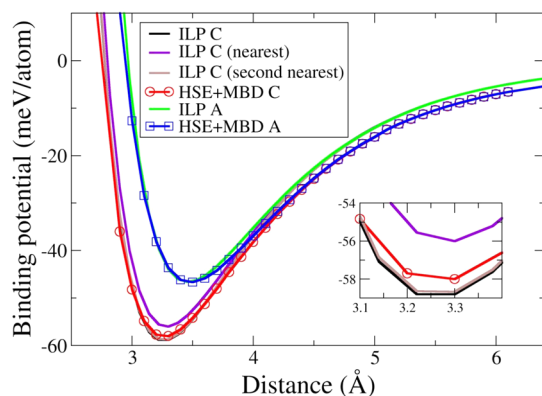
Figure 2. Binding energy curves of bulk graphene/*h*-BN alternating stacks as a function of interlayer distance. Reference HSE+MBD calculations at the optimal (C) and worst (A) stacking modes are presented in red and blue, respectively. The corresponding ILP results are presented in black and green, respectively. ILP calculations at the optimal stacking mode with only nearest (purple) and second-nearest (brown) neighboring layer interactions are also presented. Inset: zoom in on the equilibrium region of the optimally stacked system. The calculated binding energies were divided by the total number of atoms per unit-cell. Reference energies were taken as the sum of individual layer contributions.

the benzene atop HBNC system and the graphene/*h*-BN bilayer by rigidly shifting the monomers laterally at a fixed interlayer distance of 3.3 Å, are shown in Figure 3.

Fitting Procedure and Results. In the present implementation, we use the values of $d = 15.0$ and $s_R = 0.784$ for the Fermi-type short-range cutoff function in the dispersion term. We note that these values are smaller than the corresponding values used in an HSE-based Tkatchenko-Scheffler dispersion correction (20.0 and 0.96, respectively).[36,62] This results in a somewhat deeper penetration of the short-range cutoff function into the core region, reflecting the fact that the HSE functional

has a somewhat larger degree of midrange correlation than the intralayer potentials used here.

The r_{ij}^{eff} and $C_{6,ij}$ parameters are then refitted for the heterojunction. To this end, we first calculated the homonuclear r_{ii}^{eff} and $C_{6,ii}$ for the periodic graphene and *h*-BN monolayers, obtained from HSE calculations augmented by Tkatchenko-Scheffler dispersion corrections. The heteronuclear values were then obtained using the relation

$$C_{6,ij} = 2C_{6,ii}C_{6,jj} / \left(\frac{\alpha_j^0}{\alpha_i^0} C_{6,ii} + \frac{\alpha_i^0}{\alpha_j^0} C_{6,jj} \right)$$

where α_i^0 is the static polarizability of atom i.[45] Further parameter refinement then proceeded iteratively by considering the binding and sliding results alternately. Ultimately, we found it necessary to increase all calculated C_6 coefficients by ~10% for best results. All recommended parameters are summarized in Table 1.

The ILP binding-energy curves for all dimers considered, obtained using the set of parameters given in Table 1, are compared to the corresponding DFT reference results in Figure 1. As can be readily seen, the graphene/*h*-BN ILP results are in overall excellent agreement with the reference data. The maximal deviation was found for the borazine on coronene dimer (Figure 1c), where an 8.2% (0.59 meV/atom) underestimated binding energy and a 2.12% (0.07 Å) overestimated binding distance was obtained. For the periodic bilayer system (panel 1e) positioned at the C stacking mode, the ILP overestimates the binding energy by 3.2% (0.87 meV/atom) and results in a slightly increased binding distance (~0.01 Å) compared to that obtained with DFT. Numerical values of the binding energies and equilibrium distances obtained for all five systems considered, using the ILP and DFT, are provided in Table 2.

BENCHMARK TESTS

An important character of the above-developed ILP should be transferability, i.e., it should be sufficiently robust to provide an accurate description of graphene/*h*-BN systems that it was not fitted against. To examine this, we first evaluate the transferability of the obtained parametrization by considering the binding energy of a periodic (bulk) stack of alternating graphene and *h*-BN layers. The binding energy as a function of interlayer distance for this system, as calculated using HSE+MBD and the ILP for the optimal (C) and worst (A) stacking modes following the same procedure used above for the periodic bilayer system, is given in Figure 2. In this calculation, the HSE+MBD calculations are performed on a bilayer unit-cell with periodic boundary conditions applied also in the perpendicular direction. The corresponding ILP calculations are performed with a stack of 16 layers and circular boundary conditions, to allow for appropriate decay of interactions at the length of the simulation box. For the graphene/graphene and *h*-BN/*h*-BN interactions we use the Kolmogorov-Crespi[39] and *h*-BN ILP[40] potentials, respectively.

As readily seen, excellent agreement between the ILP results and the reference HSE+MBD calculations is obtained for both stacking modes also in the bulk case. Importantly, in the ILP calculations, we used the parameters obtained for the bilayer systems to describe the interactions between nonadjacent layers as well. Hence, the overall good agreement of the bulk ILP binding energy curves with the reference calculations indicates that screening of interactions between nonadjacent layers is of
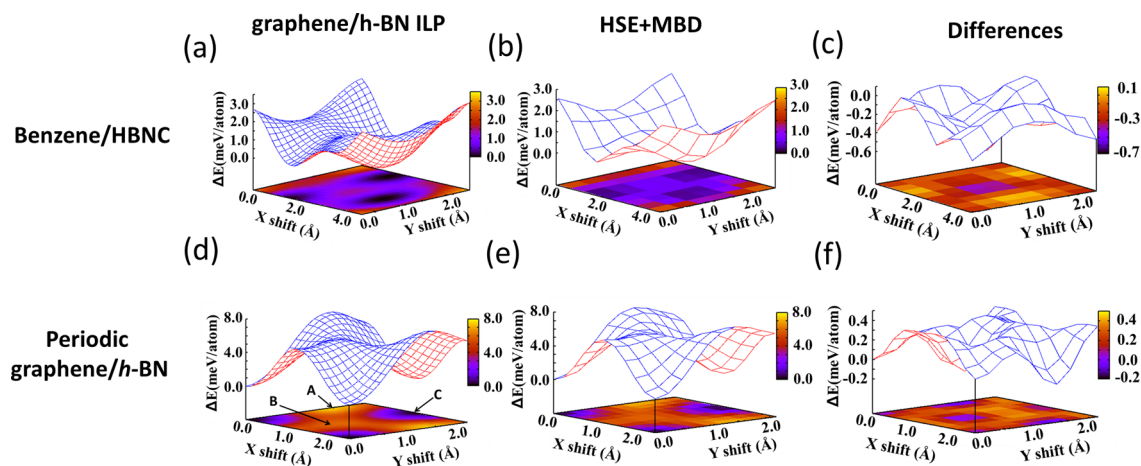
Figure 3. Interlayer sliding energy landscapes of benzene on HBNC (upper row) and a periodic graphene/h-BN bilayer (lower row), calculated using the graphene/h-BN ILP developed in this work (panels (a) and (d)), and the HSE+MBD approach (panels (b) and (e)). The differences between the ILP and DFT sliding energy landscapes are presented in panels (c) and (f). Locations of the high symmetry stacking modes of the periodic system (see Figure 1f) are marked in panel (d).

Table 1. Complete Parameter List for the Graphene/h-BN Interlayer Potential

term	parameter	value						units
		CB	CN	CH	BH	NH	HH	
dispersive	d	15.0	15.0	15.0	15.0	15.0	15.0	
	s_R	0.784	0.784	0.784	0.784	0.784	0.784	
	r_{ij}^{eff}	3.691	3.481	3.197	3.292	3.082	2.798	Å
	$C_{6,ij}$	657.408	366.955	131.989	185.686	90.589	37.870	kcal · Å^6/mol
taper	R_{cut}	16.0	16.0	16.0	16.0	16.0	16.0	Å
repulsive	α_{ij}	10.0	10.0	9.0	9.0	9.0	9.0	
	β_{ij}	3.02	3.4	2.8	2.8	2.7	2.7	Å
	γ_{ij}	1.2	1.2	20.0	20.0	20.0	20.0	Å
	ε_{ij}	0.37	0.21	0.31	0.31	0.25	0.31	kcal/mol
	C_{ij}	0.18	0.36	0.13	0.13	0.13	0.13	kcal/mol

minor importance. Furthermore, we find that the major contribution to the binding energy comes from the nearest and second-nearest neighboring layers, such that third-nearest layer interactions amount to less than 0.3% of the overall binding energy.
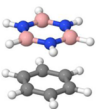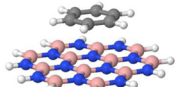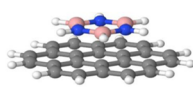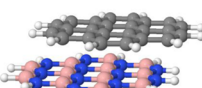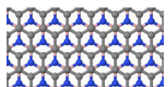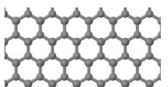
As can be seen in Figure 3, the same set of parameters also provides an excellent agreement of the calculated ILP sliding energy landscapes of the benzene/HBNC and the periodic bilayer systems with their respective reference DFT-based landscapes. Notably, the largest absolute energy difference between the ILP and DFT sliding energy surfaces obtained for the finite dimer is 0.7 meV/atom (see Figure 3c), whereas a slightly smaller absolute deviation of 0.4 meV/atom is obtained for the periodic bilayer (see Figure 3f). Furthermore, the maximal sliding energy landscape corrugation of 7.4 meV/atom, calculated for the periodic bilayer using the ILP, agrees well with the corresponding DFT reference value of 7.3 meV/atom.

Next, we focus on a more challenging application of the ILP developed in this work, which is already outside the computational feasibility scope of a DFT calculation. We consider the periodic bilayer formed by graphene and single-layered h-BN that is known to form a structural superlattice due to the intrinsic lattice constant mismatch of the two hexagonal layers.[15] We start by relaxing a graphene sheet atop a fixed h-BN single-layer forming a 24.23 × 13.99 nm^2 supercell. This system, which we denote as graphene/h-BN, has been

previously considered theoretically, computationally, and experimentally and therefore serves as an excellent testing ground for the new parametrization.[7,8,15−17,19,26,27,31] To describe the intralayer interactions in graphene we chose the Tersoff[72] potential, as parametrized in ref 73. Because this method overestimates the intralayer equilibrium C−C bond distance in graphene by ∼1.34% (yielding 1.439 Å instead of 1.42 Å), we artificially set the bond length of the fixed h-BN substrate to 1.465 Å, so as to obtain the required 1.8% interlayer lattice constant mismatch.

Figures 4a and 4b present maps of the obtained graphene/h-BN interlayer distances and the interatomic distances within the relaxed graphene layer, respectively. Clearly visible domains, characterized by optimal interlayer distance (marked in blue in panel 4a) and increased intralayer C−C bond lengths (marked in red in panel 4b) appear upon geometry optimization of the adsorbed graphene layer. In these domains, the graphene layer stretches to adapt to the underlying fixed h-BN substrate, achieving optimal C stacking at the equilibrium interlayer distance. To compensate for this, the adsorbed graphene layer forms elevated regions (marked in red in panel 4a) with compressed interatomic distances (marked in blue in panel 4b) that separate the optimally stacked domains. The maximum height variation obtained for graphene atop the fixed h-BN flat substrate was 0.23 Å, and the corresponding largest C−C bond length variations were of the order of 0.01 Å (∼0.8%). These results are consistent with previous theoretical studies[7,16,26,31]

Table 2. Binding Energies (BE) and Equilibrium Distances for All Finite and Periodic Systems Studied in Figure 1, As Obtained Using the HSE+MBD Approach and the Graphene/h-BN ILP Developed in This Work[a]

Structure	Borazine/benzene dimer		Benzene on HBNC	
	BE(meV/atom)	Eq. distance (Å)	BE(meV/atom)	Eq. distance (Å)
DFT	-5.7	3.42	-6.5	3.35
ILP	-5.6	3.44	-6.9	3.32

Structure	Borazine on Coronene		Coronene/HBNC dimer	
	BE(meV/atom)	Eq. distance (Å)	BE(meV/atom)	Eq. distance (Å)
DFT	-7.2	3.29	-12.2	3.34
ILP	-6.6	3.36	-12.2	3.37

Structure	Graphene/h-BN bilayer (C stacking)		Graphene/h-BN bilayer (A stacking)	
	BE(meV/atom)	Eq. distance (Å)	BE(meV/atom)	Eq. distance (Å)
DFT	-27.13	3.28	-21.7	3.51
ILP	-28.0	3.29	-22.3	3.48

[a]For the periodic bilayer (lower row), results for both the C (most stable) and A (least stable) stacking modes are presented.

and are in good agreement with scanning tunneling microscopy (STM) experiments that mapped the surface topography of graphene on h-BN.[8,15] Specifically, comparing the interlayer distance variation map of Figure 4a with the STM images of ref 15 reveals a very similar qualitative structure of a slightly distorted hexagonal superlattice. The experimentally measured interlayer distance variations amplitude is ~0.4 Å,[74] and the C−C bond length within the C stacked domains is found to be stretched by 2.0 ± 0.6% with respect to the elevated regions.[15] These values are somewhat larger than those obtained here from the ILP but in overall good agreement. The difference can be partially attributed to the fact that in the calculation we assume a fixed single-layered h-BN substrate, whereas in the experiment the surface region of the bulk h-BN substrate is free to deform.

To rationalize the formation of the superlattice structure, we used the recently developed local registry index (LRI) method[34] to map the degree of local interlattice commensurability in the heterogeneous bilayer system. In this method, each atom in the graphene or h-BN layer is assigned a number ranging from 0 (optimal C stacking) to 1 (worst A stacking) that quantifies its local stacking registry with respect to the underlying h-BN surface. The LRI value assigned to each atomic position is calculated from a normalized expression involving the projected overlaps between circles located at the neighboring lattice sites of the adjacent layers, averaged over the local environment. For more details on the LRI method see the Supporting Information and ref 34. Figure 4c presents the obtained LRI map of the preoptimized graphene/h-BN flat bilayer, where the blue and red colors denote regions of optimal and worst stacking modes, respectively. The LRI pattern reveals a hexagonal Moiré superlattice with lattice vector lengths that depend on the relative interlayer twist angle θ via[8] $L^M = (1 + \varepsilon)a/\sqrt{\varepsilon^2 + 2(1 + \varepsilon)[1 - \cos(\theta)]}$. Here, $a = 2.49$ Å is the lattice constant of graphene (obtained using the Tersoff[72,73] potential), and $1 + \varepsilon = 1.018$ is the ratio between the lattice constants of the two layers. In the present case, the layers are not rotated with respect to each other. Therefore, $\theta = 0°$ and the superlattice period is $L^M = 14.08$ nm (see Figure 4c). The internal structure of each supercell includes domains of nearly perfect registry, separated by reduced registry regions. Upon structural relaxation, the C−C bonds within the nearly perfect domains stretch to form a perfectly C stacked domain at the optimal interlayer distance of ~3.3 Å (Figure 4a), whereas the reduced-registry domains form the compressed elevated regions.

The corrugation of the relaxed graphene layer can be readily understood by further analysis of the LRI map of the preoptimized, flat Moiré supercell. Figure 4c shows that nearly optimal C stacking appears at the center of the supercell, but the corners obtain the A and B stacking configurations (see Figure 1f). Because the A, B, and C modes have different interlayer equilibrium distances of 3.48, 3.45, and 3.29 Å (as calculated with the ILP developed here), respectively, upon structural relaxation the graphene layer adjusts the interlayer distance according to the local stacking mode, thereby leading to the observed surface corrugation.

We now consider single-layered h-BN relaxed atop a fixed graphene substrate, a system that we denote as h-BN/graphene (see Figure 4d-f). To the best of our knowledge relaxation effects in this system have not been examined experimentally. However, the approach developed here allows for a predictive calculation. To describe the intralayer interactions of the h-BN layer we use the parametrization presented in ref 75 for the Tersoff[72] potential. Since this potential underestimates the B−N bond distance in h-BN by ~0.27% (1.442 Å), we fix the bond length of the graphene substrate at 1.4165 Å so as to maintain the required 1.8% interlayer lattice constant mismatch. We find an overall picture similar to that obtained for the above-discussed case of graphene/h-BN, the main difference being that the formation of optimal stacking regions in the relaxed h-BN layer atop the fixed graphene sheet requires B−N bond compression (Figure 4e) in order to increase commensurability with the underlying fixed graphene substrate. This is compensated by bond stretching within the surrounding elevated regions. Generally, somewhat larger regions that present nearly equilibrium interlayer distance (Figure 4d, f) are obtained along with an inverted intralayer bond-length map (Figure 4e).

Finally, we consider the case of a fully relaxed free-standing graphene/h-BN bilayer. In Figure 5 we present the LRI (panel 5a), interlayer (panel 5b) distance, and intralayer (panel 5c) C−C bond length maps obtained after fully relaxing a graphene/h-BN bilayer. As can be seen, for the free-standing system sharp domain walls develop between the optimally
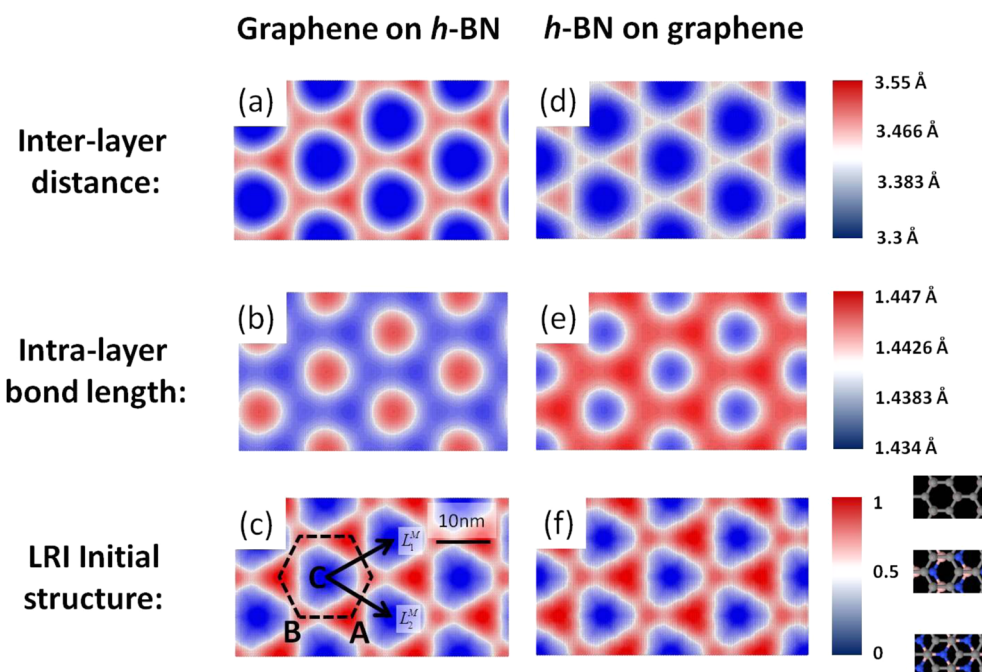
Figure 4. Relaxed graphene/fixed *h*-BN and relaxed *h*-BN/fixed graphene structures. Structural analysis of a graphene sheet relaxed atop a fixed *h*-BN sheet (left) and an *h*-BN sheet relaxed atop a fixed graphene sheet (right). Interlayer distance maps and intralayer interatomic bond-length maps of the relaxed structures are given in the top and middle panels, respectively. Local registry index (LRI) maps of the preoptimized flat bilayers appear at the bottom panels. The hexagonal Moiré supercell and three high symmetry points are marked in the bottom left panel. The false-color scale of each map is shown on the right.
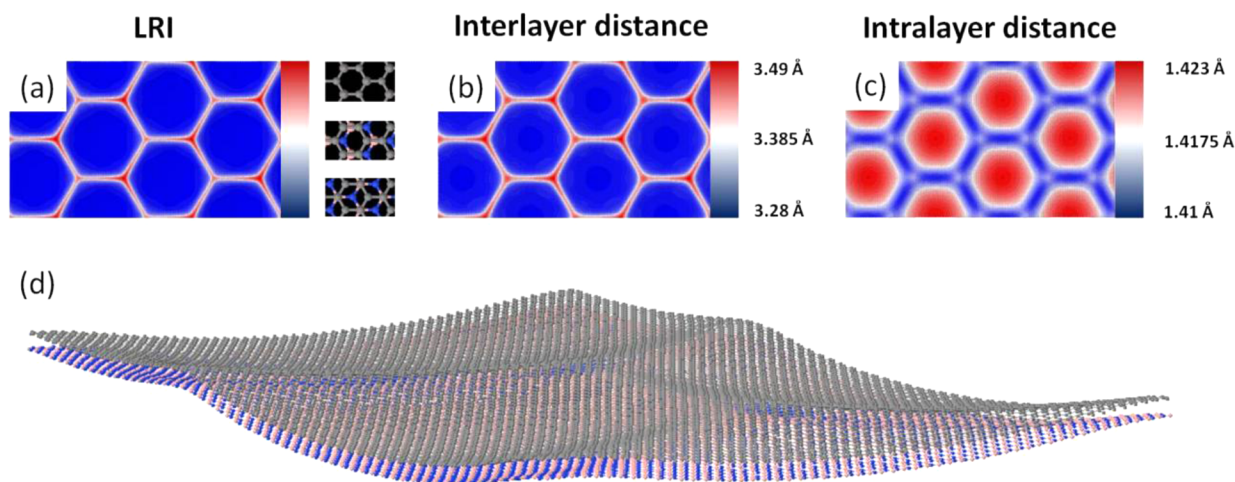
Figure 5. Fully relaxed graphene/*h*-BN free-standing bilayer. (a) Local registry index map; (b) interlayer distance map; (c) graphene intralayer distance map; and (d) overall structure of a fully relaxed, free-standing, graphene/*h*-BN bilayer. Here, we modify the equilibrium carbon−carbon bond length of the Tersoff potential from its original value of 1.439 Å to 1.416 Å in order to obtain the required 1.8% mismatch with the B−N bond length of 1.442 Å obtained with the Tersoff potential for *h*-BN.

stacked hexagonal regions. The graphene intralayer C−C bonds compress at the domain walls and stretch within the optimal stacking regions in order to accommodate the intrinsic lattice vectors mismatch of graphene and *h*-BN. Examining the relaxed structure (Figure 5d), we find that the local lattice variations are accompanied by large deformations of the whole structure, resulting in loss of planarity and the formation of a strongly corrugated surface. The surface corrugation that we obtain is of the order of 7.5 Å. When compared to the experimental height variation in the supported case (∼0.4 Å[74]), one may expect that the electronic properties of the free-standing bilayer will be strongly influenced by the structural deformations and hence

differ from those of the underlying monolayers. Furthermore, the surface corrugation is strongly dependent on interlayer twisting such that at a misfit angle of 20° the relaxed surface height variations are of the order of only ∼0.03 Å. This opens another venue for gaining control over the tribological and electronic properties of the system.

■ SUMMARY AND CONCLUSIONS

To summarize, an interlayer potential for the heterogeneous graphene/*h*-BN junction has been developed. The force-field parameters have been calibrated against reference data of binding and sliding energy profiles of several finite molecular

dimers, as well as the periodic bilayer system, obtained via screened-exchange hybrid DFT calculations augmented by many-body dispersion interactions. The ILP reproduces the DFT data with binding-energies and equilibrium distance deviations of the order of ~1 meV/atom and 0.07 Å at most (usually smaller), respectively. The transferability of the parametrization has been demonstrated by considering the binding energy of bulk graphene/h-BN alternating stacks. The potential was further benchmarked by considering the structural relaxation of the periodic graphene and h-BN heterojunction. When graphene is relaxed atop a fixed h-BN substrate, the Moiré pattern resulting from the intrinsic lattice constant mismatch of the two layers yields a corrugated surface superlattice. The structure of this superlattice is found to be in qualitative and quantitative agreement with experimental observations and with the results of previous computational studies. For single-layered h-BN relaxed atop a fixed graphene substrate, a similar picture is predicted to occur. However, unlike the case of graphene, where the C−C bonds stretch in the valleys of the corrugated surface to increase commensurability with the underlying h-BN substrate, in this case the B−N bonds compress to achieve optimal stacking with the fixed graphene surface. Upon full relaxation of a free-standing graphene/h-BN bilayer, sharp domain walls that are accompanied by a large out-of-plane deformation of the whole system emerge. This demonstrates the potential of the developed force-field to simulate structural, mechanical, tribological, and dynamical properties of layered heterostructures based on graphene and h-BN.

■ ASSOCIATED CONTENT

Ⓢ Supporting Information

The Supporting Information is available free of charge on the ACS Publications website at DOI: 10.1021/acs.jctc.6b00147.

> Description of the calculations performed to estimate the effects of basis set superposition errors, a description of the convergence settings used throughout the calculations, and the definition of the local registry index for the graphene/h-BN heterostructure (PDF)

■ AUTHOR INFORMATION

Corresponding Author
*E-mail: odedhod@tau.ac.il.
Notes
The authors declare no competing financial interest.

■ ACKNOWLEDGMENTS

■ REFERENCES

(1) Novoselov, K. S.; Castro Neto, A. H. Two-dimensional crystals-based heterostructures: materials with tailored properties. *Phys. Scr.* **2012**, *T146*, 014006.

(2) Wang, H.; Liu, F.; Fu, W.; Fang, Z.; Zhou, W.; Liu, Z. Two-dimensional heterostructures: fabrication, characterization, and application. *Nanoscale* **2014**, *6*, 12250−12272.

(3) Geim, A. K.; Grigorieva, I. V. Van der Waals heterostructures. *Nature* **2013**, *499*, 419−425.

(4) Das, S.; Robinson, J. A.; Dubey, M.; Terrones, H.; Terrones, M. Beyond graphene: progress in novel two-dimensional materials and van der Waals solids. *Annu. Rev. Mater. Res.* **2015**, *45*, 1−27.

(5) Chen, Z. G.; Shi, Z.; Yang, W.; Lu, X.; Lai, Y.; Yan, H.; Wang, F.; Zhang, G.; Li, Z. Observation of an intrinsic bandgap and Landau level renormalization in graphene/boron-nitride heterostructures. *Nat. Commun.* **2014**, *5*, 4461.

(6) Fan, Y.; Zhao, M.; Wang, Z.; Zhang, X.; Zhang, H. Tunable electronic structures of graphene/boron nitride heterobilayers. *Appl. Phys. Lett.* **2011**, *98*, 083103.

(7) Jung, J.; DaSilva, A. M.; MacDonald, A. H.; Adam, S. Origin of band gaps in graphene on hexagonal boron nitride. *Nat. Commun.* **2015**, *6*, 6308.

(8) Yankowitz, M.; Xue, J.; Cormode, D.; Sanchez-Yamagishi, J. D.; Watanabe, K.; Taniguchi, T.; Jarillo-Herrero, P.; Jacquod, P.; LeRoy, B. J. Emergence of superlattice Dirac points in graphene on hexagonal boron nitride. *Nat. Phys.* **2012**, *8*, 382−386.

(9) Dean, C. R.; Young, A. F.; Meric, I.; Lee, C.; Wang, L.; Sorgenfrei, S.; Watanabe, K.; Taniguchi, T.; Kim, P.; Shepard, K. L.; Hone, J. Boron nitride substrates for high-quality graphene electronics. *Nat. Nanotechnol.* **2010**, *5*, 722−726.

(10) Levendorf, M. P.; Kim, C. J.; Brown, L.; Huang, P. Y.; Havener, R. W.; Muller, D. A.; Park, J. Graphene and boron nitride lateral heterostructures for atomically thin circuitry. *Nature* **2012**, *488*, 627−632.

(11) Tang, S.; Wang, H.; Zhang, Y.; Li, A.; Xie, H.; Liu, X.; Liu, L.; Li, T.; Huang, F.; Xie, X.; Jiang, M. Precisely aligned graphene grown on hexagonal boron nitride by catalyst free chemical vapor deposition. *Sci. Rep.* **2013**, *3*, 2666.

(12) Ponomarenko, L. A.; Gorbachev, R. V.; Yu, G. L.; Elias, D. C.; Jalil, R.; Patel, A. A.; Mishchenko, A.; Mayorov, A. S.; Woods, C. R.; Wallbank, J. R.; Mucha-Kruczynski, M.; Piot, B. A.; Potemski, M.; Grigorieva, I. V.; Novoselov, K. S.; Guinea, F.; Fal'ko, V. I.; Geim, A. K. Cloning of Dirac fermions in graphene superlattices. *Nature* **2013**, *497*, 594−597.

(13) Dean, C. R.; Wang, L.; Maher, P.; Forsythe, C.; Ghahari, F.; Gao, Y.; Katoch, J.; Ishigami, M.; Moon, P.; Koshino, M.; Taniguchi, T.; Watanabe, K.; Shepard, K. L.; Hone, J.; Kim, P. Hofstadter's butterfly and the fractal quantum Hall effect in Moiré superlattices. *Nature* **2013**, *497*, 598−602.

(14) Dai, S.; Ma, Q.; Liu, M. K.; Andersen, T.; Fei, Z.; Goldflam, M. D.; Wagner, M.; Watanabe, K.; Taniguchi, T.; Thiemens, M.; Keilmann, F.; Janssen, G. C. A. M.; Zhu, S. E.; Jarillo-Herrero, P.; Fogler, M. M.; Basov, D. N. Graphene on hexagonal boron nitride as a tunable hyperbolic metamaterial. *Nat. Nanotechnol.* **2015**, *10*, 682−686.

(15) Woods, C. R.; Britnell, L.; Eckmann, A.; Ma, R. S.; Lu, J. C.; Guo, H. M.; Lin, X.; Yu, G. L.; Cao, Y.; Gorbachev, R. V.; Kretinin, A. V.; Park, J.; Ponomarenko, L. A.; Katsnelson, M. I.; Gornostyrev, Y. N.; Watanabe, K.; Taniguchi, T.; Casiraghi, C.; Gao, H. J.; Geim, A. K.; Novoselov, K. S. Commensurate-incommensurate transition in graphene on hexagonal boron nitride. *Nat. Phys.* **2014**, *10*, 451−456.

(16) Kumar, H.; Er, D.; Dong, L.; Li, J.; Shenoy, V. B. Elastic deformations in 2D van der Waals heterostructures and their impact on optoelectronic properties: Predictions from a multiscale computational approach. *Sci. Rep.* **2015**, *5*, 10872.

(17) Slotman, G. J.; van Wijk, M. M.; Zhao, P. L.; Fasolino, A.; Katsnelson, M. I.; Yuan, S. Effect of structural relaxation on the electronic structure of graphene on hexagonal boron nitride. *Phys. Rev. Lett.* **2015**, *115*, 186801.

(18) Mucha-Kruczyński, M.; Wallbank, J. R.; Fal'ko, V. I. Moiré miniband features in the angle-resolved photoemission spectra of graphene/hBN heterostructures. *Phys. Rev. B: Condens. Matter Mater. Phys.* **2016**, *93*, 085409.

(19) Leven, I.; Krepel, D.; Shemesh, O.; Hod, O. Robust Superlubricity in Graphene/h-BN heterojunctions. *J. Phys. Chem. Lett.* **2013**, *4*, 115−120.

(20) Wang, L. F.; Ma, T. B.; Hu, Y. Z.; Zheng, Q.; Wang, H.; Luo, J. Superlubricity of two-dimensional fluorographene/MoS_2 heterostructure: a first-principles study. *Nanotechnology* **2014**, *25*, 385701.

(21) Ansari, N.; Nazari, F.; Illas, F. Theoretical study of electronic and tribological properties of h-BNC_2/graphene, h-BNC_2/h-BN and h-BNC_2/h-BNC_2 bilayers. *Phys. Chem. Chem. Phys.* **2015**, *17*, 12908−12918.

(22) Gao, W.; Tkatchenko, A. Sliding mechanisms in multilayered hexagonal boron nitride and graphene: the effects of directionality, thickness, and sliding constraints. *Phys. Rev. Lett.* **2015**, *114*, 096101.

(23) Hod, O. Quantifying the stacking registry matching in layered materials. *Isr. J. Chem.* **2010**, *50*, 506−514.

(24) Hod, O. Interlayer commensurability and superlubricity in rigid layered materials. *Phys. Rev. B: Condens. Matter Mater. Phys.* **2012**, *86*, 075444.

(25) Hod, O. The registry Index: A quantitative measure of materials' interfacial commensurability. *ChemPhysChem* **2013**, *14*, 2376−2391.

(26) van Wijk, M. M.; Schuring, A.; Katsnelson, M. I.; Fasolino, A. Moiré patterns as a probe of interplanar interactions for graphene on h-BN. *Phys. Rev. Lett.* **2014**, *113*, 135504.

(27) Moon, P.; Koshino, M. Electronic properties of graphene/hexagonal-boron-nitride Moiré superlattice. *Phys. Rev. B: Condens. Matter Mater. Phys.* **2014**, *90*, 155406.

(28) Oz, I.; Leven, I.; Itkin, Y.; Buchwalter, A.; Akulov, K.; Hod, O. Nanotube motion on layered materials: A registry perspective. *J. Phys. Chem. C* **2016**, *120*, 4466−4470.

(29) Lee, C.; Li, Q.; Kalb, W.; Liu, X. Z.; Berger, H.; Carpick, R. W.; Hone, J. Frictional characteristics of atomically thin sheets. *Science* **2010**, *328*, 76−80.

(30) van Wijk, M. M.; Dienwiebel, M.; Frenken, J. W. M.; Fasolino, A. Superlubric to stick-slip sliding of incommensurate graphene flakes on graphite. *Phys. Rev. B: Condens. Matter Mater. Phys.* **2013**, *88*, 235423.

(31) Zhang, C.; Song, J.; Yang, Q. Periodic buckling patterns of graphene/hexagonal boron nitride heterostructure. *Nanotechnology* **2014**, *25*, 445401.

(32) Butz, B.; Dolle, C.; Niekiel, F.; Weber, K.; Waldmann, D.; Weber, H. B.; Meyer, B.; Spiecker, E. Dislocations in bilayer graphene. *Nature* **2014**, *505*, 533−537.

(33) Korhonen, T.; Koskinen, P. Peeling of multilayer graphene creates complex interlayer sliding patterns. *Phys. Rev. B: Condens. Matter Mater. Phys.* **2015**, *92*, 115427.

(34) Leven, I.; Guerra, R.; Vanossi, A.; Tosatti, E.; Hod, O. Multi-walled nanotube faceting unravelled. 2016, Submitted for publication.

(35) Marom, N.; Bernstein, J.; Garel, J.; Tkatchenko, A.; Joselevich, E.; Kronik, L.; Hod, O. Stacking and registry effects in layered materials: The case of hexagonal boron nitride. *Phys. Rev. Lett.* **2010**, *105*, 046801.

(36) Marom, N.; Tkatchenko, A.; Rossi, M.; Gobre, V. V.; Hod, O.; Scheffler, M.; Kronik, L. Dispersion interactions with density-functional theory: Benchmarking semiempirical and interatomic pairwise corrected density functionals. *J. Chem. Theory Comput.* **2011**, *7*, 3944−3951.

(37) Hod, O. Graphite and hexagonal boron-nitride have the same interlayer distance. Why? *J. Chem. Theory Comput.* **2012**, *8*, 1360−1369.

(38) Blumberg, A.; Keshet, U.; Zaltsman, I.; Hod, O. Interlayer Registry to Determine the Sliding Potential of Layered Metal Dichalcogenides: The Case of 2H-MoS_2. *J. Phys. Chem. Lett.* **2012**, *3*, 1936−1940.

(39) Kolmogorov, A. N.; Crespi, V. H. Registry-dependent interlayer potential for graphitic systems. *Phys. Rev. B: Condens. Matter Mater. Phys.* **2005**, *71*, 235415.

(40) Leven, I.; Azuri, I.; Kronik, L.; Hod, O. Inter-layer potential for hexagonal boron nitride. *J. Chem. Phys.* **2014**, *140*, 104106.

(41) Reguzzoni, M.; Fasolino, A.; Molinari, E.; Righi, M. C. Potential energy surface for graphene on graphene: *Ab initio* derivation, analytical description, and microscopic interpretation. *Phys. Rev. B: Condens. Matter Mater. Phys.* **2012**, *86*, 245434.

(42) Tkatchenko, A.; DiStasio, R. A., Jr.; Car, R.; Scheffler, M. Accurate and efficient method for many-body van der Waals interactions. *Phys. Rev. Lett.* **2012**, *108*, 236402.

(43) Ambrosetti, A.; Reilly, A. M.; DiStasio, R. A., Jr.; Tkatchenko, A. Long-range correlation energy calculated from coupled atomic response functions. *J. Chem. Phys.* **2014**, *140*, 18A508.

(44) Lennard-Jones, J. E.; Dent, B. M. Cohesion at a crystal surface. *Trans. Faraday Soc.* **1928**, *24*, 92−108.

(45) Tkatchenko, A.; Scheffler, M. Accurate Molecular Van Der Waals Interactions from Ground-State Electron Density and Free-Atom Reference Data. *Phys. Rev. Lett.* **2009**, *102*, 073005.

(46) de Vos Burchart, E. Ph.D. Thesis, Delft University of Technology, 1992.

(47) We note that for periodic systems long-range cutoff terms may introduce computational inaccuracies that require careful convergence tests. For such systems infinite summation techniques may provide an appropriate alternative.

(48) Here, we used a stretched unit-cell, where the graphene and h-BN share the same lattice constant of 2.48 Å to avoid the need for calculating large supercells exhibiting a Moiré pattern resulting from the 1.8% intrinsic lattice mismatch of the relaxed graphene and h-BN layers. Because the reference DFT calculations and the ILP parametrization procedure are performed using the same geometries and because each layer is stretched by less than 1% from its relaxed structure, we expect the effect of using a stretched unit-cell with a fixed intralayer bond length on the obtained ILP parameters to be negligible.

(49) Marom, N.; Tkatchenko, A.; Scheffler, M.; Kronik, L. Describing both dispersion interactions and electronic structure using density functional theory: The case of metal−phthalocyanine dimers. *J. Chem. Theory Comput.* **2010**, *6*, 81−90.

(50) Heyd, J.; Scuseria, G. E.; Ernzerhof, M. Hybrid functionals based on a screened Coulomb potential. *J. Chem. Phys.* **2003**, *118*, 8207−8215.

(51) Heyd, J.; Scuseria, G. E. Assessment and validation of a screened Coulomb hybrid density functional. *J. Chem. Phys.* **2004**, *120*, 7274−7280.

(52) Heyd, J.; Scuseria, G. E. Efficient hybrid density functional calculations in solids: Assessment of the Heyd-Scuseria-Ernzerhof screened Coulomb hybrid functional. *J. Chem. Phys.* **2004**, *121*, 1187−1192.

(53) Heyd, J.; Scuseria, G. E.; Ernzerhof, M. Erratum: "Hybrid functionals based on a screened Coulomb potential" [J. Chem. Phys. 118, 8207 (2003)]. *J. Chem. Phys.* **2006**, *124*, 219906−219901.

(54) Barone, V.; Hod, O.; Peralta, J. E.; Scuseria, G. E. Accurate Prediction of the Electronic Properties of Low-Dimensional Graphene Derivatives Using a Screened Hybrid Density Functional. *Acc. Chem. Res.* **2011**, *44*, 269−279.

(55) Barone, V.; Peralta, J. E. Magnetic Boron Nitride Nanoribbons with Tunable Electronic Properties. *Nano Lett.* **2008**, *8*, 2210−2214.

(56) Berseneva, N.; Krasheninnikov, A. V.; Nieminen, R. M. Mechanisms of postsynthesis doping of boron nitride nanostructures with carbon from first-principles simulations. *Phys. Rev. Lett.* **2011**, *107*, 035501.

(57) Zhu, J.; Bhandary, S.; Sanyal, B.; Ottosson, H. Interpolation of Atomically Thin Hexagonal Boron Nitride and Graphene: Electronic Structure and Thermodynamic Stability in Terms of All-Carbon Conjugated Paths and Aromatic Hexagons. *J. Phys. Chem. C* **2011**, *115*, 10264−10271.

(58) Liu, Y.; Wu, X.; Zhao, Y.; Zeng, X. C.; Yang, J. Half-Metallicity in Hybrid Graphene/Boron Nitride Nanoribbons with Dihydrogenated Edges. *J. Phys. Chem. C* **2011**, *115*, 9442−9450.

(59) Du, A.; Sanvito, S.; Li, Z.; Wang, D.; Jiao, Y.; Liao, T.; Sun, Q.; Ng, Y. H.; Zhu, Z.; Amal, R.; Smith, S. C. Hybrid Graphene and Graphitic Carbon Nitride Nanocomposite: Gap Opening, Electron−

Hole Puddle, Interfacial Charge Transfer, and Enhanced Visible Light Response. *J. Am. Chem. Soc.* **2012**, *134*, 4393−4397.

(60) Gobre, V. V.; Tkatchenko, A. Scaling laws for van der Waals interactions in nanostructured materials. *Nat. Commun.* **2013**, *4*, 2341.

(61) Ambrosetti, A.; Alfè, D.; DiStasio, R. A., Jr.; Tkatchenko, A. Hard Numbers for Large Molecules: Toward Exact Energetics for Supramolecular Systems. *J. Phys. Chem. Lett.* **2014**, *5*, 849−855.

(62) Kronik, L.; Tkatchenko, A. Understanding Molecular Crystals with Dispersion-Inclusive Density Functional Theory: Pairwise Corrections and Beyond. *Acc. Chem. Res.* **2014**, *47*, 3208−3216.

(63) Maurer, R. J.; Ruiz, V. G.; Tkatchenko, A. Many-body dispersion effects in the binding of adsorbates on metal surfaces. *J. Chem. Phys.* **2015**, *143*, 102808.

(64) Bučko, T.; Lebègue, S.; Gould, T.; Ángyán, J. G. Many-body dispersion corrections for periodic systems: An efficient reciprocal space implementation. *J. Phys.: Condens. Matter* **2016**, *28*, 045201.

(65) Blood-Forsythe, M. A.; Markovich, T.; DiStasio, R. A., Jr.; Car, R.; Aspuru-Guzik, A. Analytical Nuclear Gradients for the Range-Separated Many-Body Dispersion Model of Noncovalent Interactions. *Chem. Sci.* **2016**, *7*, 1712.

(66) Hsing, C.-R.; Cheng, C.; Chou, J.-P.; Chang, C.-M.; Wei, C.-M. Van der Waals interaction in a boron nitride bilayer. *New J. Phys.* **2014**, *16*, 113015.

(67) Mostaani, E.; Drummond, N. D.; Fal'ko, V. I. Quantum monte carlo calculation of the binding energy of bilayer graphene. *Phys. Rev. Lett.* **2015**, *115*, 115501.

(68) Hariharan, P. C.; Pople, J. A. The Influence of Polarization Functions on Molecular Orbital Hydrogenation Energies. *Theor. Chim. Acta (Berl.)* **1973**, *28*, 213−222.

(69) Frisch, M. J.; Trucks, G. W.; Schlegel, H. B.; Scuseria, G. E.; Robb, M. A.; Cheeseman, J. R.; Scalmani, G.; Barone, V.; Mennucci, B.; Petersson, G. A.; Nakatsuji, H.; Caricato, M.; Li, X.; Hratchian, H. P.; Izmaylov, A. F.; Bloino, J.; Zheng, G.; Sonnenberg, J. L.; Hada, M.; Ehara, M.; Toyota, K.; Fukuda, R.; Hasegawa, J.; Ishida, M.; Nakajima, T.; Honda, Y.; Kitao, O.; Nakai, H.; Vreven, T.; Montgomery, J. A., Jr.; Peralta, J. E.; Ogliaro, F.; Bearpark, M.; Heyd, J. J.; Brothers, E.; Kudin, K. N.; Staroverov, V. N.; Kobayashi, R.; Normand, J.; Raghavachari, K.; Rendell, A.; Burant, J. C.; Iyengar, S. S.; Tomasi, J.; Cossi, M.; Rega, N.; Millam, J. M.; Klene, M.; Knox, J. E.; Cross, J. B.; Bakken, V.; Adamo, C.; Jaramillo, J.; Gomperts, R.; Stratmann, R. E.; Yazyev, O.; Austin, A. J.; Cammi, R.; Pomelli, C.; Ochterski, J. W.; Martin, R. L.; Morokuma, K.; Zakrzewski, V. G.; Voth, G. A.; Salvador, P.; Dannenberg, J. J.; Dapprich, S.; Daniels, A. D.; Farkas, Ö.; Foresman, J. B.; Ortiz, J. V.; Cioslowski, J.; Fox, D. J. *Gaussian 09, Revision A.02*; Wallingford, CT, 2009.

(70) Havu, V.; Blum, V.; Havu, P.; Scheffler, M. Efficient O(N) integration for all-electron electronic structure calculation using numeric basis functions. *J. Comput. Phys.* **2009**, *228*, 8367−8379.

(71) Blum, V.; Gehrke, R.; Hanke, F.; Havu, P.; Havu, V.; Ren, X.; Reuter, K.; Scheffler, M. *Ab initio* molecular simulations with numeric atom-centered orbitals. *Comput. Phys. Commun.* **2009**, *180*, 2175−2196.

(72) Tersoff, J. Modeling solid-state chemistry - interatomic potentials for multicomponent systems. *Phys. Rev. B: Condens. Matter Mater. Phys.* **1989**, *39*, 5566−5568.

(73) Lindsay, L.; Broido, D. A. Optimized Tersoff and Brenner empirical potential parameters for lattice dynamics and phonon thermal transport in carbon nanotubes and graphene. *Phys. Rev. B: Condens. Matter Mater. Phys.* **2010**, *81*, 205441.

(74) Yang, W.; Chen, G.; Shi, Z.; Liu, C.-C.; Zhang, L.; Xie, G.; Cheng, M.; Wang, D.; Yang, R.; Shi, D.; Watanabe, K.; Taniguchi, T.; Yao, Y.; Zhang, Y.; Zhang, G. Epitaxial growth of single-domain graphene on hexagonal boron nitride. *Nat. Mater.* **2013**, *12*, 792−797.

(75) Sevik, C.; Kinaci, A.; Haskins, J. B.; Çağın, T. Characterization of thermal transport in low-dimensional boron nitride nanostructures. *Phys. Rev. B: Condens. Matter Mater. Phys.* **2011**, *84*, 085409.